JOURNAL OF MATERIALS SCIENCE 30 (1995) 6105–6112

Laser surface melting and alloying of type 304L stainless steel

Part II *Corrosion and wear resistance properties*

O. V. AKGUN, O. T. INAL*
Department of Materials and Metallurgical Engineering, New Mexico Institute of Mining and Technology, Socorro, NM 87801, USA

Laser surface melting (LSM) and alloying (LSA) of type 304L stainless steel with molybdenum and tantalum have been studied for improvement of corrosion and wear-resistance properties. These properties were seen to be affected by the presence of δ-ferrite, produced by the high cooling rate in LSM, as well as by compositional modifications introduced in molybdenum- and tantalum-alloyed LSA layers. Passivation and pitting-resistance properties were seen to be enhanced with increase in δ-ferrite content in LSM samples. Excellent corrosion properties were observed for the molybdenum-alloyed layer. The tantalum-alloyed layer had similar corrosion properties to those achieved with LSM of 304L. The improvement of abrasive wear resistance of the laser-processed samples with increase in hardness was found to be very small compared to the untreated alloy.

1. Introduction

In the last two decades, laser surface modification of metals and alloys has found increasing use in engineering applications to enhance surface properties through the alteration of surface chemistry and structure. Laser processing techniques, such as laser surface heating (LSH), laser surface melting (LSM), and laser surface alloying (LSA), are widely used for surface-layer modifications. In LSH, the surface is heated above its transformation temperature, and then cooled rapidly to room temperature to form a hardened surface layer [1]. In LSM, a high-power laser beam rapidly melts a thin surface layer, and the rest of the material provides self-quenching at cooling rates of up to 10^4–10^8 K s^{-1}. This modified microstructure, melted and rapidly solidified, improves the corrosion and wear resistance of some alloys [2–8].

For some alloys these properties cannot be improved by LSM alone because of the associated low temperatures of phase transformation, for example in austenitic stainless steels, or because of the absence of suitable phase transformation, and, in these cases, LSA becomes an alternative to LSM. In LSA an alloying element is introduced into the substrate surface by different techniques, such as coating, particle injection, etc., and then melted with a high-energy laser beam [4, 9–12]. After mixing and resolidification, a thin surface layer is produced with different chemical composition and properties from the substrate material.

In Part I, we showed that LSM of 304L increased the δ-ferrite content in the microstructure up to 10 vol % and through LSA with molybdenum and tantalum of 304L, δ-ferrite became the major phase [12]. In this study, the effect of increased δ-ferrite content on corrosion and wear-resistance properties were investigated.

2. Experimental procedure

Laser source, materials, alloying, chemical analysis, optical and transmission electron microscopy were explained in Part I [12].

2.1. Scanning electron microscopy

The surfaces of stress corrosion cracked (SCC) and abraded wear samples were analysed using a Hitachi model HHS-2R scanning electron microscope (SEM) equipped with a Tracor Northern Model TN 5400 energy dispersive spectrometer X-ray microanalyser (EDX).

2.2. Microhardness testing

Hardness changes after laser surface melting and alloying were determined with a Leco M-400 Vickers microhardness tester. Hardness measurements were taken from the transverse section of the laser surface melted and alloyed layers. The load used was 200 gf for all samples, maintained for 15 s.

2.3. Corrosion tests

Corrosion tests were carried out in a Princeton Applied Research (PAR) standard corrosion cell with

*Author to whom all correspondence should be addressed.

0022–2461

a PAR Model 173 potentiostat/galvanostat and PAR Model 175 universal programmer. The potentiostat was equipped with a PAR Model 376 logarithmic current converter. The output was recorded with a PAR $X-Y$ recorder Model RE0074. A saturated calomel electrode (SCE) was used as a reference electrode.

The samples, with an area of 1 cm^2, were cut from the laser-melted and alloyed plates, and the surfaces were polished with 600 grit SiC paper to remove any extraneous layer. Solutions were deaerated with nitrogen gas for 1 h, and then were immersed in the solution and deaerating continued for a further 0.5 h. Corrosion potentials were measured after 1 h immersion of the samples. This was followed by potentiodynamic polarization at a scan rate of 1 $mV\,s^{-1}$. Pitting potential is defined here as a potential at which current density increases rapidly. Passivation and pitting tests were carried out in 1N H_2SO_4 and 3.5 wt % NaCl solutions, respectively. These tests were performed at room temperature.

Weight-loss determination for as-received, LSM and LS molybdenum- and tantalum-alloyed samples were carried out in 10% $FeCl_3 \cdot 6H_2O$ solution. Approximately 3 cm^2 area of the LSM or alloyed layer was sliced from the substrate, and care was taken to ensure that any unmelted or unalloyed substrate material was removed. Exact weight loss was measured for the laser-treated layers. They were weighed with an accuracy of 0.001 g before and after immersion in the test solution. Sheet samples were suspended in the solution by teflon tape that passed through a hole on the top of the sample. Tests were conducted for 96 h and in a constant-temperature bath of 22 °C. After the test was completed, samples were cleaned in an ultrasonic cleaner to remove corrosion products. Each sample was examined with an optical microscope.

The stress corrosion cracking (SCC) test was only conducted for the as-received and laser surface melted samples. The initial composition and mechanical properties for the alloy used in the SCC test are given in Table I. Laser surface melting was performed at a laser power of 4 kW and a scan speed of 7 $mm\,s^{-1}$ under nitrogen gas. This gave a melt depth of 700 μm. The laser surface melting process for the SCC samples is shown schematically in Fig. 1. Cylindrical specimen dimensions were 12.7 cm length and 0.76 cm diameter. Melt paths were made parallel to the major axis of the sample to avoid any notch effect due to melt paths during testing. To ensure 50% overlapping for the melt paths, the specimen was rotated 10.8° about its major axis after each melt path was completed. As a result, the melted zone covered 32% of the total cross-sectional area of the specimen.

Following laser surface melting, surface roughness of the samples was removed by polishing with 600 grit SiC paper; the samples were then cleaned with methanol in the ultrasonic cleaner and washed with distilled water. The test solution was neutral 0.5 wt % NaCl at a temperature of 95 °C. During testing, temperature was controlled by immersed heaters and the solution was exposed to ambient air through a condenser. An MTS-810 type mechanical testing machine was used for the tests. Strain rate was $1.6 \times 10^{-6}\,s^{-1}$. The test was started after the specimen was brought into contact with the solution. All fracture surfaces were examined with SEM.

TABLE I (a) Chemical composition and (b) mechanical properties (annealed at 1065 °C) of as-received AISI 304 stainless steel used for SCC test

(a)

C	Mn	Si	S	P	Cr	Ni	Mo
0.072	1.46	0.68	0.022	0.024	18.19	9.02	0.56

Co	Cu	N	Fe
0.10	0.34	0.078	Bal

(b)

UTS (MPa)	0.2% YS (MPa)	% EL (in)	% RA	BHN
653	376.5	46.4	76.5	180

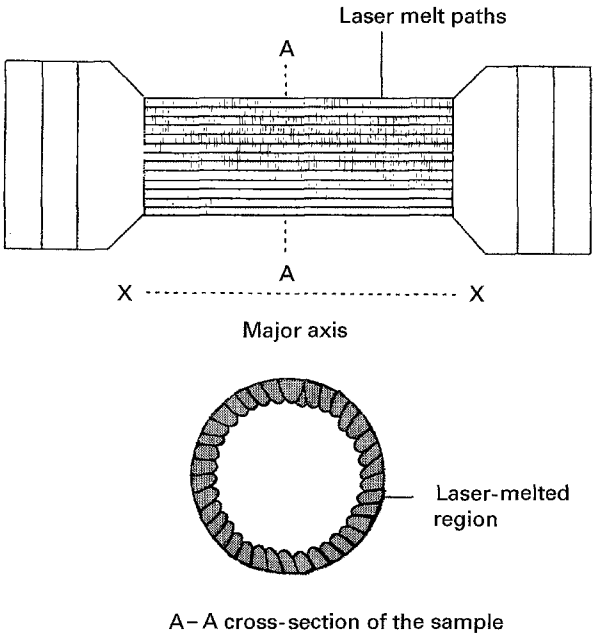

Figure 1 Laser surface melting of SCC test samples.

2.4. Wear tests

Dry sand–rubber wheel abrasion tests were performed by Falex Corporation, Aurora, IL, on as-received, LSM, and LSA samples according to ASTM Standard Practice G-65 Procedure A. The 2.5 cm × 7.5 cm × 1.25 cm samples were prepared, and final surface polishing was made with 600-grid SiC sand-paper.

Samples were weighed before and after the test to determine the weight loss, and then the volume loss was determined.

3. Results and discussion

3.1. Corrosion resistance tests

To determine the technological usefulness of laser surface melting and alloying (with molybdenum or tantalum) on 304L austenitic stainless steel, corrosion

TABLE II Passivation potentials and currents of the samples in 1N H_2SO_4 solution (deaerated and 25 °C)

Alloy	Depth (μm)	E_{cor} (mV versus SCE)	i_{crit} (μA cm^{-2})
As-received	–	−450	655
LSM[a]	0	−350	91
	80	−348	32
	170	−350	50
	250	−347	23
	400	−342	28
	510	−331	26
LSM[b]	650	−326	21
Mo-alloyed	–	−307	0
Ta-alloyed	–	−303	10

[a] At the surface.
[b] At the maximum melt depth.

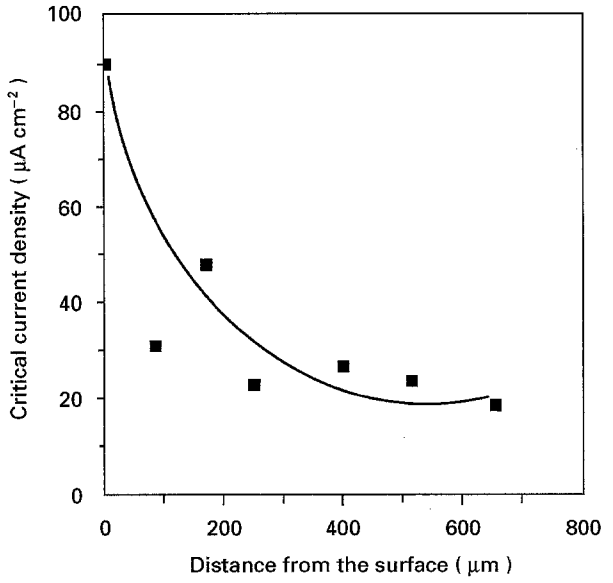

Figure 2 Changing of critical current densities in the melted layer.

resistance tests were performed. Passivation, pitting, and weight-loss tests were conducted on as-received, laser surface melted, and alloyed (molybdenum or tantalum) samples, while the stress corrosion cracking test was performed only for as-received and laser surface melted samples.

3.1.1. Laser surface melted 304L

Surface melting decreased the critical current density for passivation significantly compared to the as-received substrate, and the corrosion potential moved 100 mV in the noble direction for the laser-treated sample (Table II). δ-ferrite content in the melted zone was observed to increase toward the boundary between the melted zone and the substrate [12]. The effect of increasing δ-ferrite content on passivation behaviour of the LSM layer was investigated by removal of successive layers of 80–100 μm from the surface (Table II). The critical current density for passivation was observed to decrease, and reached its lowest value at maximum melt depth, indicating easy passivation behaviour with increasing δ-ferrite content (Fig. 2).

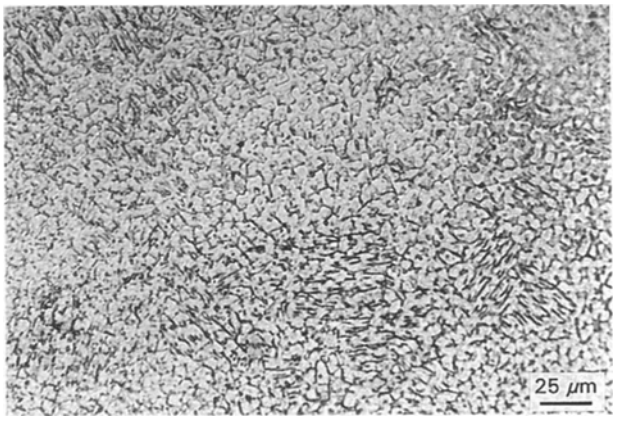

Figure 3 δ-ferrite network in LSM type 304L microstructure.

TABLE III Pitting and corrosion potentials of the samples tested in 3.5 wt % NaCl deaerated solution at 25 °C

Alloy	E_C[a]	E_P[a]
As-received	−163	85
LSM[b]	−230	275
LSM[c]	−290	445
Mo-alloyed	−174	None
Ta-alloyed	−125	225

[a] mV versus SCE.
[b] At the surface.
[c] 400 μm layer removed.

The improvement in corrosion-resistance properties, easy passivation and increase in pitting potential, observed for LSM can be attributed to an increasing δ-ferrite, redistribution and/or removal of MnS inclusions, and primary δ-ferrite solidification mode.

As seen in Fig. 3, the increase in δ-ferrite content in the laser-melted layer leads to the formation of a semi-continuous network of this phase in the microstructure. It is well known that the chromium content in rapidly solidified 304 stainless steel is higher in δ-ferrite than in the austenite phase [13]. On the other hand, the chromium content in the alloy does not change following laser melting. Therefore, a possible explanation for the decrease in critical current density for passivation in LSM samples is an increase in the chromium content in the oxide film as a result of the semi-continuous δ-ferrite network in the microstructure. This effect is clearly observed in our experimental results, shown in Fig. 2, where critical current density for passivation decreases sharply and reaches its lowest value at maximum melt depth.

The pitting potential increased substantially following laser surface melting (Table III). Pitting tests were conducted on the sample before and after the removal of about 400 μm of the melted layer after each test. The highest pitting potential was recorded at the maximum melt depth where the δ-ferrite content was highest.

Pitting corrosion resistance of LSM type-304 was previously investigated by T. R. Jervis *et al.* [10]. They observed the removal or redistribution of inclusions in the laser-melted layer of 304 stainless steel and

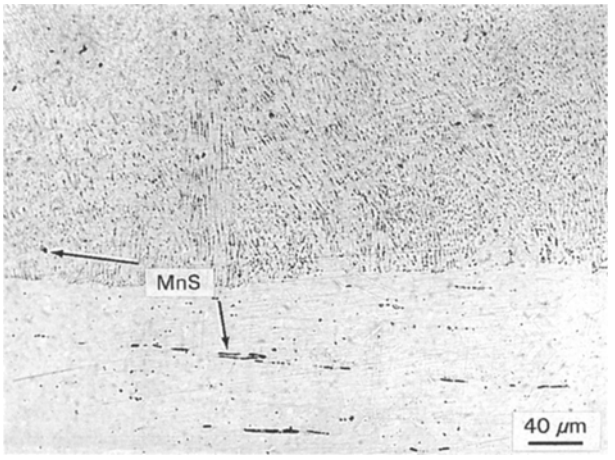

Figure 4 Distribution of MnS inclusions in substrate and melted region of LSM type 304L.

suggested this to improve pitting corrosion resistance. Redistribution of MnS inclusions is observed in our samples, and is shown in Fig. 4. This optical micrograph is taken of a surface parallel to the rolling direction, wherein elongated MnS inclusions are clearly seen. In the laser-melted region, in contrast, MnS particles are fewer and are in the form of very small inclusions.

Another factor that could be contributory in the present case is the solidification mode experienced and its effect on impurity segregation. It is well documented in the literature that solubility of sulphur in δ-ferrite is higher than in austenite [14]. During solidification of primary δ-ferrite, relatively less sulphur is rejected into the liquid. This results in less sulphur segregation into the δ-ferrite/γ boundary. Therefore, a higher pitting resistance would be achieved if a primary δ-ferrite solidified structure is formed in the laser-melted layer of 304 stainless steel, because of the simultaneous trapping of sulphur and removal and/or redistribution of MnS in the melted layer. The amount of MnS formed would be considerably reduced if the primary solidification phase is δ-ferrite. This has been confirmed by La Barbera *et al.* [13] who determined quantitatively the MnS distribution in electron-beam surface-melted 304 stainless steel. Their results indicate that, as the MnS content in the melted layer decreased with melt depth, δ-ferrite content increased and reached a maximum value there.

Weight-loss tests, conducted in neutral 10% $FeCl_3 \cdot 6H_2O$ solution, indicate higher weight loss for the laser surface melted samples than the as-received ones (Table IV). There are two possible explanations for this excessive weight loss. The first one, which also applies to both as-received and tantalum-alloyed samples, is that corrosion potentials of these samples in ferric chloride solution are higher than their pitting corrosion potentials. The second explanation for the higher corrosion rate observed in LSM samples could be caused by galvanic corrosion. Because the microstructure of the laser-melted layer contains a network of δ-ferrite phase, with a higher chromium content, a galvanic cell with the austenite phase (containing less chromium) in a highly oxidizing ferric chloride solution could lead to more metal dissolution.

TABLE IV Weight loss in $FeCl_3 \cdot 6H_2O$ solution for 96 h at 22 °C

Alloy	($g\,m^{-2}\,d^{-1}$)	(%)
As-received	23.64	6.3
LSM	33.04	11.3
Mo-alloyed	0	0
Ta-alloyed	29.11	7.2

The following observations were also made on the laser-melted and as-received samples tested in 3.5 wt % NaCl solution. First, pit density for the LSM samples is found to be lower at maximum melt depth. Also, most of the pits are located on the surface of minimum melt depth and in overlapped regions. This could possibly suggest easy pit-forming inclusions segregating to these regions and the surface; this has also been observed elsewhere [11]. One very important observation is that pit density is higher in the laser-melted samples than the as-received ones, but pit sizes are much larger for the as-received samples.

Table V shows the result of slow strain rate stress corrosion cracking (SCC) tests on the as-received and LSM samples, tested in air and 0.5 wt % NaCl solution. LSM processing increased only the yield and ultimate tensile strengths; however, reduction in area, elongation, and time to failure, characteristic indications of SCC, were reduced for laser surface melted samples tested both in air and in 0.5 wt % NaCl solution.

3.1.2. Laser surface molybdenum-alloyed 304L

Molybdenum alloying of 304L stainless steel drastically improved the corrosion properties tested in this study, namely, passivation, pitting, and weight loss.

The alloy spontaneously passivated (no active peak visible) in deaerated 1N H_2SO_4 solution, and the corrosion potential, E_{corr}, shifted to the noble direction as compared to the as-received and LSM samples (Table II). Also, there was no pitting potential observed up to oxygen evolution potential (Table III). The molybdenum-alloyed layer showed zero weight loss in a highly aggressive 10% ferric chloride solution (Table IV).

The above results suggest that molybdenum was uniformly distributed in the alloyed layer. In addition, intermetallic phases such as sigma, chi and Laves phases, which have a deleterious effect on the localized corrosion resistance of molybdenum-alloyed stainless steels [15, 16], were not seen to form in our molybdenum-alloyed samples. These factors resulted in improved corrosion resistance.

It should be clear that the improvement in pitting resistance of molybdenum-alloyed samples strongly depends on molybdenum distribution between the phases. Therefore, the nature of the solid-state transformation from δ-ferrite to austenite becomes very critical. It seems that solid-state transformation in

TABLE V Comparison of SCC test results of as-received and LSM samples tested in 0.5 wt % NaCl solution at 95 °C (strain rate 10^{-6} s^{-1})

Sample	YS[a](MPa)	UTS[b](MPa)	RA[c](%)	E[d](%)	TTF[e](h)
304 As-received	305.6	530.5	74.8	43	154
304 LSM	381	581	70	36	139
	25% (+)[f]	9.5% (+)	6.4% (−)[g]	16.3% (−)	9.7% (−)

[a] Yield strength.
[b] Ultimate tensile strength.
[c] Reduction in area.
[d] Elongation.
[e] Time to failure.
[f] (+) increase.
[g] (−) decrease.

molybdenum-alloyed sample is less likely to be diffusion-controlled, even though the sample is exposed to a continuous higher heat input during laser alloying. This is because any diffusion-controlled transformation results in large compositional variation between parent and product phases. In our case, it would have meant poor pitting resistance for the molybdenum-alloyed sample; this is contrary to our findings.

The improved pitting properties for laser surface molybdenum-alloyed type 304 stainless steel was reported by McCafferty and Moore [4]. The alloy composition that contained 9 wt % Mo did not pit in 0.1 M NaCl solution. More importantly, similar results were observed in the present study even with 4.33 wt % Mo in the alloyed layer.

Excellent corrosion properties observed for molybdenum-alloyed samples can be attributed to primary δ-ferrite solidification mode and the presence of molybdenum in the austenite phase [12]. Previous conventional welding studies on steels containing molybdenum, such as AISI 316 or 317 with primary austenitic solidification mode, showed molybdenum segregation to interdentritic regions and reduction of pitting resistance at much lower values than that of the parent alloy of the same composition [17, 18]. Heavy pit formations were observed at molybdenum-depleted dendrite centres. Nakao *et al.* [18] demonstrated that these welds can regain their pitting resistance through laser surface melting. They attributed this improvement to the partition of molybdenum and chromium to the austenite phase due to rapid solidification. It is very clear that not only does the molybdenum content in the alloy influence the pitting resistance, but also that its distribution between the phases is a primary factor as well. Laser surface melting or alloying ensures minimum segregation of alloying species, because of the high cooling rates that can be achieved, and this, in turn, was observed to lead to property enhancements detailed here.

3.1.3. Laser surface tantalum-alloyed 304L sample

Corrosion results indicate that tantalum alloying only improved the passivation behaviour of 304L by moving E_{corr} in the more noble direction and by lowering the critical current density for passivation in 1N H_2SO_4 solution (Table II). Other corrosion properties did not improve much in comparison to other alloys. For example, pitting potential in 3.5 wt % NaCl solution is only slightly better than for the as-received 304L stainless steel (Table III). The tantalum-alloyed layer also showed poor performance in 10% ferric chloride solution similar to the LSM material (Table IV).

The following points can be argued to characterize the poor corrosion performance of tantalum-alloyed layers. First, tantalum has less solubility in both austenite and δ-ferrite phases; second, the tantalum content in our alloyed layers is close to 7 wt %; thus the excess amount of tantalum must be contained in tantalum-rich phases and/or precipitates [12]. From weight-loss experiments, it seems likely that galvanic cells possibly formed between these tantalum precipitates and regions depleted of tantalum, and this accelerated metal dissolution in ferric chloride solution.

3.2. Wear resistance test

Abrasive wear tests were conducted on the as-received, LSM, and LSA samples. Table VI shows the results of dry-sand abrasive wear tests. They all exhibit similar weight losses, although the tantalum-alloyed sample, which is the hardest one among them, has the lowest wear loss. Consistent with these test results, the abraded surfaces of all samples show continuous grooves indicating almost no resistance to movement of abrasive particles during testing (Fig. 5). It is clear that the wear mechanism observed for the samples is the formation of grooves, which are produced by shearing, ploughing or chipping of hard particles and further detachment of the materials from the edges of these grooves by repeated unidirectional motion of the abrasive particles.

Hardness evaluations made for the longitudinal and transverse sections of abraded surfaces proved that hardness was increased in each case following wear tests (Table VII). These increases were about 9% and 5% for molybdenum- and tantalum-alloyed samples, respectively. However, higher hardness increases, up to 50%, were measured for the LSM and as-received samples. These hardness measurements were taken as close to the abraded surface as possible. Furthermore,

TABLE VI Dry sand–rubber wheel abrasion test results

	AR	LSM	LS–Mo	LS–Ta
Mass loss (g)	2.1	2.13	2.08	2.02
(S.D.) ±	0.037	0.034	0.047	0.04
Density (g cm^{-3})	7.82	7.83	7.93	8.43
Volume loss (mm^3)	268.5	272.1	262.3	239.6
Wheel diameter (in.)[a]	8.498	8.533	8.575	8.484
(S.D.) ±	0.093	0.024	0.001	0.056
Adjusted volume loss (mm^3)[b]	283.9	286.9	275.8	253.2

[a] After test.

[b] Measured volume loss $\times \frac{\text{wheel diameter before test (9 in)}}{\text{wheel diameter after test}}$.

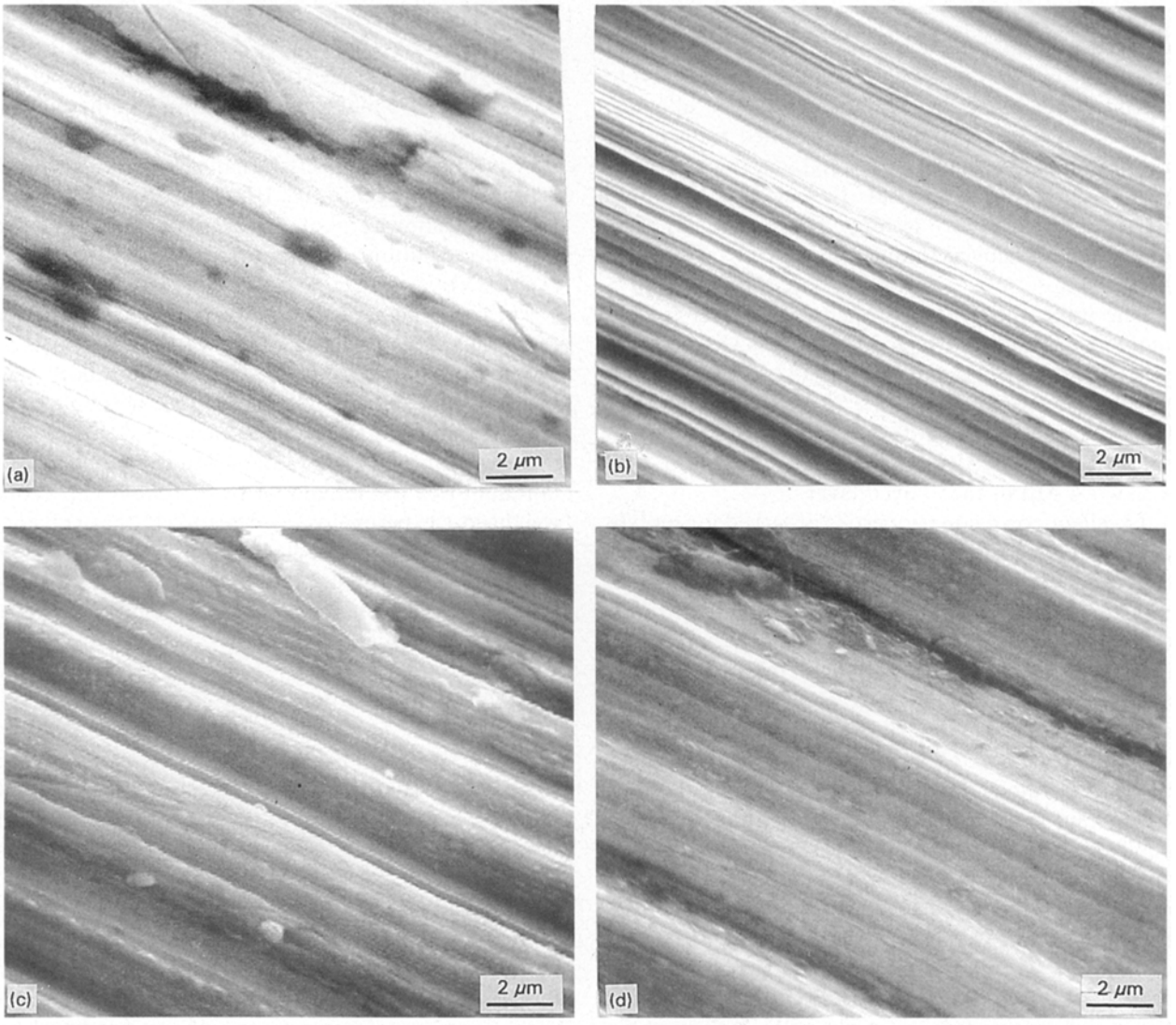

Figure 5 Scanning electron micrographs of the abrasive wear test samples: (a) AR, (b) LSM, (c) LS molybdenum-alloyed and (d) LS tantalum-alloyed.

they decayed to original hardness values within about a 5 mm distance from the wear surface.

It is reported that wear resistance of austenitic stainless steels is high in abrasion, and this is attributed to the higher work-hardening rate of these alloys [19]. The present test results also show a high work-hardening rate for type-304L austenitic stainless steel. The higher work-hardening behaviour of as-received and LSM samples is also evident from their surface morphologies (Fig. 5a, b). These samples lose their ductility because of higher work-hardening, which causes harder debris formation. These debris particles are easily removed, which results in a smooth surface morphology.

However, there was only a little work-hardening observed for molybdenum- and tantalum-alloyed samples (Table VII). This is because, in both samples, bcc δ-ferrite is the major phase. In bcc

TABLE VII Hardness test results of the samples before and after wear test

	As-received	LSM	Mo-alloyed	Ta-alloyed
Hardness before wear test (VHN)	200 ± 2	220 ± 10	304 ± 31	345 ± 20
Hardness after wear test (VHN)	285 ± 15	275 ± 18	331 ± 5	362 ± 8
Wear-test-induced hardening (%)	42.5	25	9	5

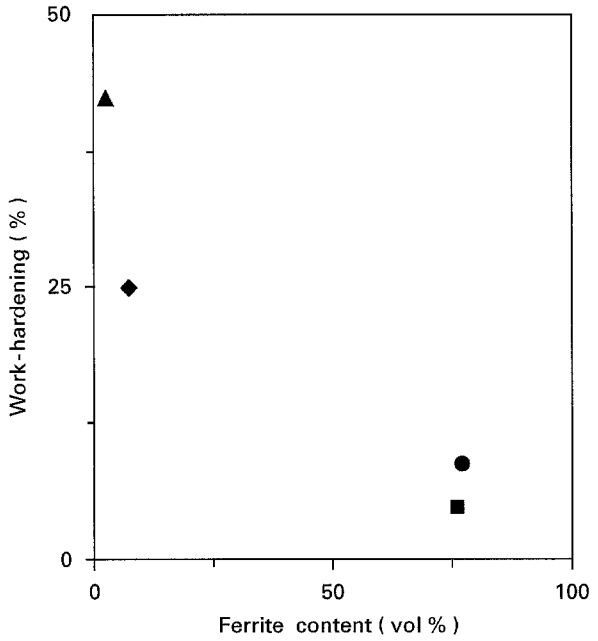

Figure 6 The effect of ferrite content on work-hardening of the samples: (■) LS Ta, (●) LS Mo, (◆) LSM, (▲) as-received.

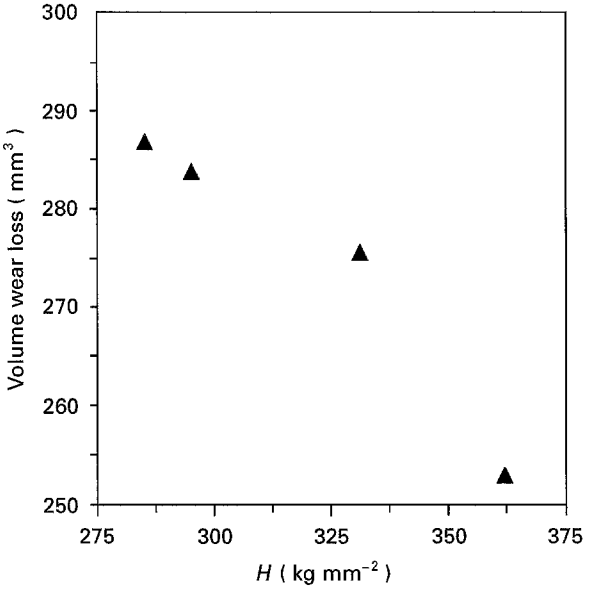

Figure 7 The change of volume wear loss with hardness (hardness values measured after the wear test).

metals, dislocation cross-slip is much easier as compared to fcc metals; this gives rise to a low work-hardening rate for bcc metals. Fig. 6 shows the change of work-hardening with volume per cent of δ-ferrite. The work-hardening decreases sharply with increasing δ-ferrite content.

Fig. 7 shows the relationship between wear volume and hardness of the samples after the wear test. As predicted by theory [20], wear loss is inversely related to hardness. These hardness values are taken after the wear test, and therefore reflect the work-hardening effect for the samples. For example, an LSM sample that had a 10% higher hardness initially than an as-received sample showed the highest wear loss. This is because LSM material exhibits less work-hardening as compared to the as-received.

Allen *et al.* [19] demonstrated that a 45% cold reduction increased the hardness of type 304L stainless steel by almost 75%. On the other hand, the strain levels at the worn surfaces were higher than for the conventional deformation process [21]. These observations possibly explain the origin of the higher hardness that we observed in our as-received sample. Eyre [16] indicated that the maximum hardness produced by wear should be considered, rather than the hardness of the unworn surface, to judge the enhancement of wear resistance in a material. Thus, higher hardnesses for our alloyed samples before the test may not be critical for a comparison of the improvement in this property because the increases among them after the test were so small, as compared to the LSM and as-received samples.

4. Conclusions

1. General observations. Dry-sand abrasive wear resistance of the laser-processed samples was found to be the same as that of the as-received alloy. Improvement in abrasion resistance with hardness was very small.

2. Laser surface melting.

(a) The corrosion properties of passivation and pitting were improved. The improvements are attributed to primary δ-ferrite solidification mode and redistribution of MnS inclusions. Critical current density for passivation decreased with increase in δ-ferrite content. Pitting potential was higher at maximum melt depth where δ-ferrite content was higher. A higher weight loss was determined in 10% ferric chloride solution.

(b) SCC resistance of LSM was found to be slightly lower than that of the as-received alloy.

3. Laser surface alloying with molybdenum. The corrosion properties of passivation and pitting were greatly improved. There was no pit formation in 3.5 wt % NaCl solution, and no weight loss in ferric chloride solution. This suggests no molybdenum depletion in the austenite phase.

4. Laser surface alloying with tantalum. The corrosion properties of passivation, pitting and weight

loss were found to be similar to those of the LSM material indicating there is no tantalum-alloying contribution to these properties.

Acknowledgement

The support of this study by EPRI under contract RP2426-39 is gratefully acknowledged.

References

1. S. BHATTACHARYYA and F. D. SEEMAN, "Laser Processing of Materials", edited by K. Mukherji and J. Mazumder (AIME, New York, 1985) p. 211.
2. T. R. ANTHONY and H. E. CLINE, *J. Appl. Phys.* **49** (1978) 1248.
3. J. B. LUMSDEN, D. S. GNANAMUTHU and R. J. MOORES, in "Fundamental Aspects of Corrosion Protection by Surface Modification", edited by E. McCafferty, C. R. Clayton and J. Oudar (Electrochemical Society, Pennington, NJ, 1984) p. 122.
4. E. Mc CAFFERTY and P. G. MOORE, *J. Electrochem. Soc.* **133** (1986) 1090.
5. T. R. JERVIS, D. J. FRYDRYCH and D. R. BAER, *Mater. Lett.* **6** (1988) 225.
6. T. R. JERVIS and J-P. HIRVONEN, *Wear* **6** (1991) 225.
7. O. V. AKGUN and O. T. INAL, *J. Mater. Sci. Eng.* **27** (1992) 2147.
8. J. D. AYERS and T. R. TUCKER, *Thin Solid Films* **73** (1980) 201.
9. J. D. AYERS, R. J. SCHAEFER and W. P. ROBEY, *J. Metals* **33** (1981) 19.
10. T. R. JERVIS, J-.P. HIRVONEN and M. NASTASI, *J. Mater. Res.* **3** (1988) 1104.
11. V. NAIK, S. M. CHAUDHARI, S. M. KANETKAR, S. B. OGALE, A. P. B. SINHA and C. K. GUPTA, *Thin Solid Films* **83** (1990) 197.
12. O. V. AKGUN and O. T. INAL, *J. Mater. Sci.* **30** (1995) ●●●●.
13. A. LA BARBERA, S. MARTELLI, A. MIGNONE, F. PIERDOMINICI, M. VITTORI and G. LULLI, in Proceedings of the European Conference on "Laser Treatment of Materials", edited by Barry L. Mordike (DGM, Oberursel, Germany, 1986) p. 79.
14. T. ZACHARIA, S. A. DAVID, J. M. VITEK and T. DEBROY, *Metall. Trans.* **20A** (1989) 957.
15. A. J. SEDRIKS, *Corrosion* **42** (1986) 376.
16. T. S. EYRE, "Tribology International", Vol. 9 (IPC Science and Technology Press, Guildford, UK, 1976).
17. A. GARNER, *Corrosion* **35** (1979) 108.
18. Y. NAKAO, K. NISHIMOTO and W. P. ZANG, in "The 5th International Symposium of the Japan Welding Society" (1990) p. 935.
19. C. ALLEN, A. BALL and B. E. PROTHEREO, *Wear* **74** (1981–1982) 287.
20. M. M. KHRUSHCHOV, in "Proceedings of the Conference on Lubrication and Wear" (Institute of Mechanical Engineers, London, 1957) p. 655.
21. M. A. MOORE, R. C. D. RICHARDSON and D. G. ATTWOOD, *Metall. Trans.* **3** (1972) p. 2485.

Received 4 January 1994
and accepted 7 June 1995